Prediction of hysteresis losses by an advanced vector hysteresis stop model with threshold surfaces

Xiao Xiao, Fabian Müller, Martin Marco Nell and Kay Hameyer
Institute of Electrical Machines, RWTH Aachen University, Aachen, Germany

Received 9 November 2021
Revised 11 January 2022
Accepted 15 March 2022

Abstract

Purpose – The ordinary vector hysteresis stop model with constant threshold values is not able to prohibit the hysteretic property after the saturation correctly. This paper aims to develop an improved vector hysteresis stop model with threshold surfaces. This advanced anisotropic vector hysteresis stop model can represent the magnetic saturation properties and the hysteresis losses under alternating and rotating magnetizations.

Design/methodology/approach – By integrating anhysteretic surfaces into the elastic element of a vector hysteresis stop model, the anisotropy of the permeability of an electrical steel sheet can be represented. Instead of the commonly used constant threshold value for plastic elements of the hysteresis model, threshold surfaces are applied to the stop hysterons. The threshold surfaces can be derived directly from measured alternating major loops of the material sample. By saturated polarization, the constructed threshold surfaces are vanishing. In this way, the reversible magnetic flux density is in the same direction of the applied magnetic flux density. Thus, the saturation properties are satisfied.

Findings – Analyzing the measurements of the electrical steel sheets sample obtained from a rotational single sheet tester shows that the clockwise (CW) and counter-CW (CCW) rotational hysteresis losses decrease by saturated flux density. At this state, instead of the domain wall motion, the magnetization rotation is dominant in the material. As a result, the hysteresis losses, which are related to the domain wall motion, are vanished near the saturation. In one stop operator, the plastic element represents the hysteresis part of the model. Integrating threshold surface into the plastic element, the hysteresis part can be modified to zero near the saturation to represent the saturation properties.

Originality/value – The results of this work demonstrate that the presented vector hysteresis stop model allows simulation of anisotropic hysteresis effects, alternating and rotating hysteresis losses. The parameters of the hysteresis model are determined by comparing the measured and modeled minor loops in different alternating magnetization directions. With the identified parameters, the proposed model is excited with rotated excitations in CW and CCW directions. The rotated hysteresis losses, derived from the model, are then compared with those experimentally measured. The modified vector stop model can significantly improve the accuracy of representing hysteresis saturations and losses.

Keywords Soft magnetic materials, Magnetic hysteresis, Material modelling, Magnetic anisotropy, Magnetic nonlinearity, Magnetic saturation

Paper type Research paper

The authors thanks Dr Klaus Kuhnen of Robert Bosch GmbH for sharing his experiences in hysteresis modeling. The German Research Foundation (DFG) supported this work within the Research project number 373150943 “Vector hysteresis modeling of ferromagnetic materials”.

COMPEL - The international journal for computation and mathematics in electrical and electronic engineering

0332-1649
DOI 10.1108/COMPEL-11-2021-0434

1. Introduction

The vector stop model gained growing interest in recent years, as the anisotropic magnetic properties can be modeled with less computational cost and measurement efforts. The model is derived from continuum mechanics and relies on thermodynamic consistency by using stop operators with mechanical analogy (Bergqvist *et al.*, 1997). The original formulation of this hysteresis model is developed from the Prandtl–Ishilinskii model (Bobbio *et al.*, 1997), which is well established in continuum mechanics. Using rheological elements to characterize the material properties, a vector stop operator is divided into an elastic and a plastic element. As it possesses a constitution relationship of magnetic field strength to magnetic flux density $\boldsymbol{H}(\boldsymbol{B})$, the material model can be directly incorporated into the vector potential formulation in the finite element method without inverse efforts.

To predict the field solutions in electrical machines more accurately, the anisotropy of the materials is considered by material modeling. This is because in non-oriented electrical steel sheets, the magnetic properties of the permeability and coercive fields differ depending on the magnetization directions (Chwastek, 2013) (Martin *et al.*, 2015). The material modeling is becoming more complicated when the material is excited with rotating magnetic fields which can be found in rotating machines and T-joints of transformers. The magnetic behavior of electrical steel excited by uniaxial fields varies to the behavior under rotating fields in iron losses (Bergqvist and Engdahl, 1994) (Torre *et al.*, 2006) (Matsuo, 2008). The hysteresis losses under rotational excitations decrease for high inductions in contrast to unidirectional excitations, where the losses further increase. The reason why this difference occurs, is because the magnetic materials exhibit nonlocal memory. The state of the hysteresis loops is determined by the magnetic domain structure at that moment. In this way, the history of the material together with the excitation values determine the state value of hysteresis. When the material reaches its saturation, the domain structure is swept away by large excitation fields. Thus, the material is independent to the history at saturation (Bertotti, 1998). The reversible anhysteretic part is then dominant and the phase lag between $\boldsymbol{B}$ and $\boldsymbol{H}$ tends to become zero near the saturation. To represent the hysteresis losses accurately and physical correctly, the irreversible part should be vanished near the saturation.

Constructing the plastic element with a constant threshold value as in an ordinary stop model (Leite *et al.*, 2005), the presented properties of rotating hysteresis losses cannot be satisfied. There are stop models proposed to predict the losses with input dependent weighting functions (Matsuo and Shimasaki, 2007) or with modified stop operators considering the saturation (Matsuo, 2008). In this paper, this is improved by applying a threshold model for the plastic elements of the vector hysteresis stop model.

2. Measurements

An electrical steel sheet sample M330-35 (2.4 Wt.% Si) is measured by a rotational single sheet tester, where alternating and rotating excitations are imposed to the sample. The sample has a width and length of 60 mm × 60 mm and a thickness of 0.334 mm. More details about the measurement topologies can be found in Bavendiek *et al.* (2019). In the case of alternating excitations, the measurements are performed for every 10° from 0° to 180°. The data are smoothed and interpolated with cubic smooth spline. The alternating measurements exhibit x-axis and y-axis symmetries. Thus, the hysteresis loops from 0° to 80° are averaged with the loops from 180° to 100° to ensure this property.

The alternating and rotating measurements are performed at 50 Hz and the stop model is a static vector hysteresis model. The classic field caused by eddy currents at this rate should be removed.

The eddy current induced classic field can be calculated as follows (Bertotti, 1998):

$$H_{classic}(t) = \frac{\sigma d^2}{12}\frac{dB}{dt} = \frac{\sigma d^2}{12}\frac{\Delta B(\Delta t)}{\Delta t}, \quad (1)$$

where the electrical conductivity is $\sigma = 1.10^7$S/m, the thickness is $d = 0.334$ mm and the time step is t. Moreover, one period contains 1,000 data points, $\Delta t = T/1000$. A comparison of measurements and processed data in x direction is shown in Figure 1. To show the data clearly, only hysteresis loops in the first quadrant are illustrated in Figure 1. After removing this dynamic effect, the processed hysteresis curves are slimmer than the original measured hysteresis data. By means of averaging the data from 0° to 80° with the data from 180° to 100°, the measured data are resulted in one clear hysteresis loop in the symmetrical directions. This is implemented in Figure 1 as processed data in black.

3. Vector hysteresis stop model

In this work, the advanced vector hysteresis stop model is used to characterize the anisotropic hysteretic behavior and to represent the hysteresis losses under unidirectional and rotating excitations.

On the microscopic scale, the hysteresis losses correspond to the pinning of Bloch walls due to crystallographic defects and structural disorder inside the material. This pinning effect causes further magnetic Barkhausen jumps with discontinuous changes in the flux density. The Barkhausen jumps are irreversible and behave as a stochastic nature during the magnetization process (Bertotti, 1998). Using a threshold value to denote the pinning field is presented in Bergqvist (1997). To give a more realistic picture by representing this random feature, the hysteresis model is constructed by connecting a number of vectorized stop operators in parallel. The weight ω of each stop operator describes its contribution to the entire system. The vector hysteresis stop model is then capable to represent clockwise

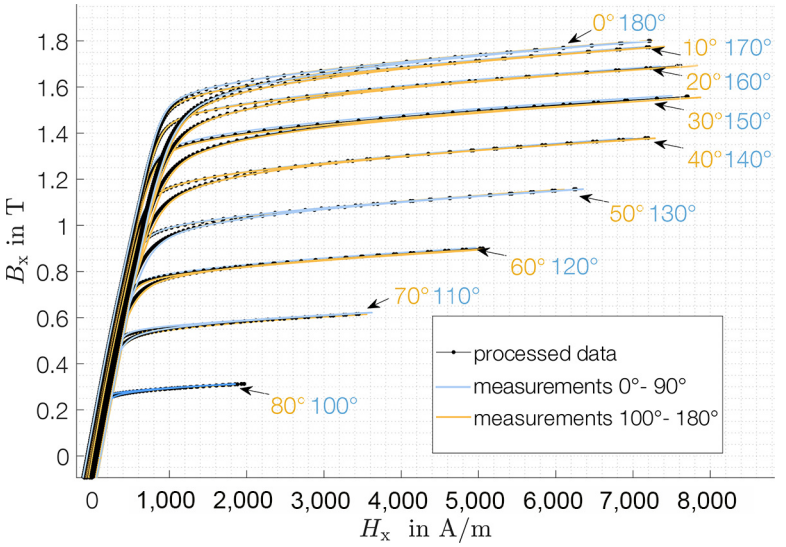

Figure 1. The measured major loops of the sample M330-35 (2.4 Wt.% Si) from 0° to 180° in steps of 10° in comparison with processed data in x direction

(CW)-oriented alternating hysteresis loops with an input of the magnetic flux density $\boldsymbol{B}$ and an output of the magnetic field strength $\boldsymbol{H}$.

3.1 Construction of a vectorized stop operator with elastic and plastic components

A stop operator is constructed by the series connection of one elastic and one plastic element (Krejčí, 1996). The elastic spring element implements the reversible characteristics of the magnetization process and the plastic dry friction element depicts the irreversible Barkhausen jumps with energy dissipation.

In this work, the anisotropic magnetic properties can be represented by integrating the anhysteretic anisotropic surfaces into the elastic components of the stop model. Instead of using the classical Langevin function and arctangent function to describe the magnetization curve as in (Krejčí, 1996) (Bastos *et al.*, 2018), the anhysteretic characteristics of the vector hysteresis model are derived from major loops in magnetization directions from 0° to 180° in steps of 10°. The threshold surfaces $\boldsymbol{R}$ represent the yield constraints for plastic elements. The details about construction of threshold surfaces are explained in the next section.

A general mathematical formulation for the n-th stop operator is given as:

$$\boldsymbol{S}_n = \boldsymbol{B}_{\mathrm{re}}{}^{t} = \begin{cases} \boldsymbol{\Omega}_n & \text{if } |\boldsymbol{R}_{\mathrm{temp\_}n}{}^{-1}\boldsymbol{\Omega}_n| < 1 \\ \boldsymbol{R}_{\mathrm{temp\_}n}\dfrac{\boldsymbol{\Omega}_n}{|\boldsymbol{\Omega}_n|} & \text{if } |\boldsymbol{R}_{\mathrm{temp\_}n}{}^{-1}\boldsymbol{\Omega}_n| \geq 1 \end{cases}, \tag{2}$$

where $\boldsymbol{\Omega}_n = \mathrm{d}\boldsymbol{B} + \boldsymbol{S}_n{}^{t-1}$, $\mathrm{d}\boldsymbol{B} = \boldsymbol{B}^{t} - \boldsymbol{B}^{t-1}$ and $\boldsymbol{R}_{\mathrm{temp\_}n}$ is the threshold diagonal matrix of the friction element of the n-th stop operator (Leite *et al.*, 2005). When the condition $|\boldsymbol{R}_{\mathrm{temp\_}n}{}^{-1}\boldsymbol{\Omega}_n| < 1$ satisfies, means that the state of model is inside the yield surface and remains unchanged. Otherwise, the response of the model is plastic and evaluated with the threshold $\boldsymbol{R}_n$ in the direction of $\boldsymbol{\Omega}_n$.

The parameter $\boldsymbol{S}_n{}^{t-1}$ is the state value of the n-th hysteron from the previous time step, which represents the history of the vector stop hysteresis model. As the hysteresis phenomenon depends not only on the input flux density $\boldsymbol{B}^{t}$ at the time instance but also on the values attained at previous time (Bertotti, 1998), the future evolution of hysteresis curve is fully determined.

3.2 Modified Vector stop model with threshold model

The plastic elements of the stop operators are modified with an input dependent threshold model to attain the nature of alternating and rotating hysteresis losses. The threshold model $\boldsymbol{R}(\boldsymbol{B})$ is derived from the measured $\boldsymbol{B}(\boldsymbol{H})$ major loop in rolling direction with:

$$\begin{cases} \boldsymbol{H}_{\boldsymbol{rev}}(\boldsymbol{B}) = \left(\boldsymbol{H}_{\boldsymbol{asd}}(\boldsymbol{B}) + \boldsymbol{H}_{\boldsymbol{des}}(\boldsymbol{B})\right)/2 \\ \boldsymbol{H}_{\boldsymbol{irr}}(\boldsymbol{B}) = \left(\boldsymbol{H}_{\boldsymbol{asd}}(\boldsymbol{B}) - \boldsymbol{H}_{\boldsymbol{des}}(\boldsymbol{B})\right)/2 \\ \boldsymbol{R}(\boldsymbol{B}) = \boldsymbol{H}_{\boldsymbol{rev}}^{-1}(\boldsymbol{H}_{\boldsymbol{irr}}) \end{cases}, \tag{3}$$

where the $\boldsymbol{H}_{\mathrm{asd}}$ is the ascending curve and $\boldsymbol{H}_{\mathrm{des}}$ is the descending curve of the hysteresis major loop. The reversible magnetization characteristic $\boldsymbol{H}_{\mathrm{rev}}(\boldsymbol{B})$ is the approximated anhysteretic curve and the $\boldsymbol{H}_{\mathrm{irr}}(\boldsymbol{B})$ describes the irreversible magnetic field. The obtained $\boldsymbol{R}(\boldsymbol{B})$ curve is shown in Figure 2.

Furthermore, the $\boldsymbol{R}(\boldsymbol{B})$ curve is extrapolated to saturation induction of the material with cubic spline. Exceeding the induction $\boldsymbol{B}$ the saturation of the material, the $\boldsymbol{R}(\boldsymbol{B})$ is set as zero.

At the range of saturation, the Barkhausen jumps will not occur anymore. As the threshold of a friction element represents the pinning field related to the Barkhausen effects, it is also expected to decline with increased amplitude of applied external induction B as depicted in Figure 3.

Rotating the obtained $\boldsymbol{R}(\boldsymbol{B})$ curve from 0° to 90° and transforming it in cartesian coordinates, a threshold surface in the first quadrant is created as shown in Figure 3(a). A full isotropic threshold surface is then modeled based on the symmetry of the x- and y-axes as illustrated in Figure 3(b).

Using five stop operators to represent the magnetic properties, the constructed isotropic threshold surfaces for each operator are shown in Figure 4. The vector hysteresis stop model is calculated from equation:

$$\boldsymbol{H}(\boldsymbol{B}) = \sum_{\boldsymbol{n}=1}^{N} \boldsymbol{w}_{\boldsymbol{n}} \boldsymbol{H}(\boldsymbol{S}_{\boldsymbol{n}}). \tag{4}$$

This equation states that the stop operator $\boldsymbol{S}_n(\boldsymbol{R}_{\text{temp\_}n})$ and the weight of each stop operator w_n together determine the form and accuracy of the hysteresis loops. Thus, the distribution and scaling of the threshold surface for each operator is determined experimentally. In order that by low inductions enough hysterons can be activated for minor loops, a third order is used to describe the distribution of n-th threshold surface. The distribution is calculated with equation:

$$\boldsymbol{R}_{\text{temp\_}n} = \left(\frac{\boldsymbol{R}(\boldsymbol{B}) \cdot n}{3}\right)^{3}. \tag{5}$$

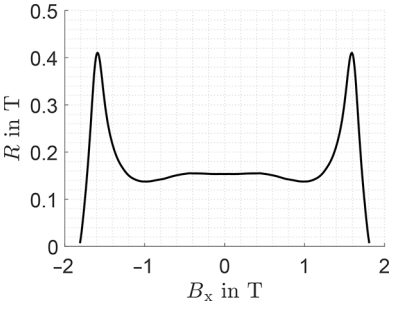

Figure 2.
The threshold curve $R(B)$ derived from the reversible and irreversible curves in the magnetization direction in 0°

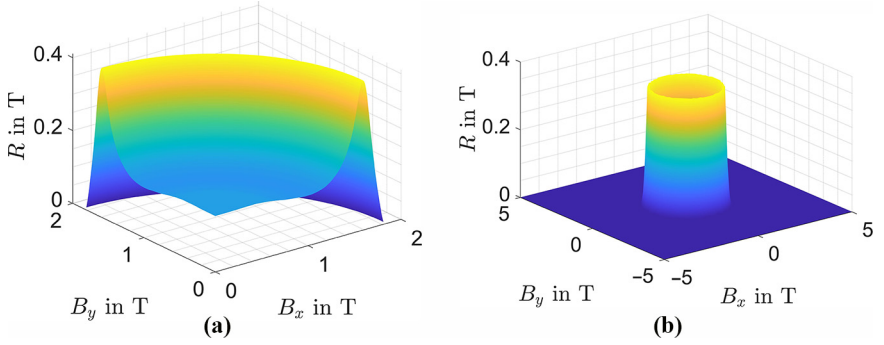

Figure 3.
Modeled threshold surfaces in first quadrant a) and a schematic illustration of the full isotropic threshold surface b)

Each time step, the threshold value is interpolated from the corresponding n-th threshold surface $\boldsymbol{R}_{\text{temp\_}n}(B_x(t),B_y(t))$ of the n-th stop operator.

4. Parameter identification and validation of vector hysteresis stop model

The measured minor loops in 0°, 30°, 60° and 90° are used for the parameter identification. Modeling with five stop hysterons, there are five weights to be identified. The first weight for the first hysteron is always equal to one, as it describes the contribution of the anhysteretic curve to the entire system (Xiao *et al.*, 2020). Applying the least-squares method, the weights can be determined by minimizing the errors between the simulation results from the model and the measurements. The identified weights are shown in Table 1.

The same identification and simulation procedures are also performed for stop models with classic constant threshold. The simulated results against the measured alternating data in 0° are illustrated in Figure 5. From this figure an improvement of accuracy on the knee range of the hysteresis curve, by applying the threshold surface for the plastic elements of stop model, can be observed.

This work mainly concerns predicting hysteresis losses with stop model. The numeric experiments are processed under alternating and rotating excitations, the accordingly calculated hysteresis losses are then compared with the measured losses. The hysteresis losses density P, referenced to the mass, can be derived by the following equation (Zhu and Koh, 2017):

$$\boldsymbol{P} = \frac{1}{\boldsymbol{T}\boldsymbol{\rho}}\int_0^{\boldsymbol{T}}\left(\boldsymbol{H}_{\boldsymbol{x}}\frac{\mathrm{d}\boldsymbol{B}_{\boldsymbol{x}}}{\mathrm{d}\boldsymbol{t}} + \boldsymbol{H}_{\boldsymbol{y}}\frac{\mathrm{d}\boldsymbol{B}_{\boldsymbol{y}}}{\mathrm{d}\boldsymbol{t}}\right)\mathrm{d}\boldsymbol{t}, \tag{6}$$

where T denotes the time period and H_x, H_y, B_x, B_y are the modeled magnetic field strength and flux density to the x and y directions, respectively. The mass density is given by $\rho = 7650\,\mathrm{kg/m^3}$.

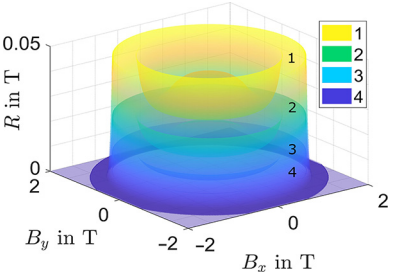

Figure 4.
Constructed threshold surfaces $R_{\text{temp\_}n}$ for each stop operator with a distribution

Table 1.
Identified weights for vector stop model with five stop operators to simulate the magnetic properties of electrical steel M330-35

w_1	w_2	w_3	w_4	w_5
1	1.8651	3.2577	1.1595	1.0913

As the alternating measurements are performed from 0° to 90°, hysteresis losses density are calculated in each direction from the modelled data by vector stop model with constant threshold value and with threshold surface. Furthermore, the derived hysteresis losses are averaged in 10 directions and compared with the averaged measured data. A comparison of the modelled averaged data to the measured alternating hysteresis losses averaged in the excitation directions from 0° to 90° is shown in Figure 6. The alternating losses are increased monotonically with the induction $\boldsymbol{B}_{\mathrm{amp}}$. The simulated hysteresis

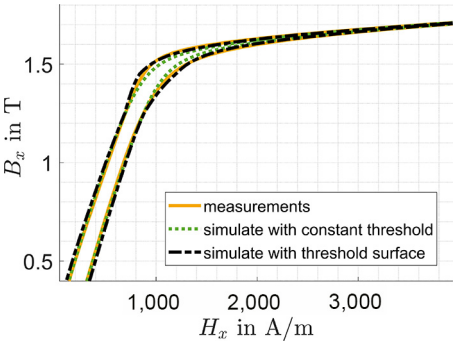

Figure 5.
Comparison of measured and simulated hysteresis loops with constant threshold value and with threshold surface under alternating excitation in 0°

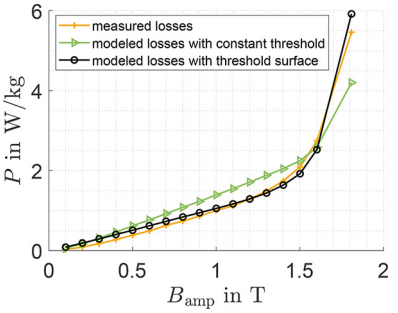

Figure 6.
A comparison between the averaged measured and simulated alternating hysteresis losses density of the material M330-35 (2.4 Wt.% Si) versus the applied unidirectional inductions with an amplitude from 0.1 T to 1.8 T in the direction from 0° to 90°

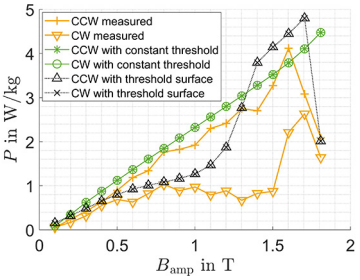

Figure 7.
Comparison of measured rotating hysteresis losses with simulated losses of the material M330-35 (2.4 Wt.% Si) versus the applied rotating flux density in CW and CCW directions

losses exhibit less anisotropy than the measured losses, which can be improved by applying a yield condition for the stop model in future study. The modeled losses with constant threshold show similar process as the losses simulated with threshold surface. Though, the simulated losses with constant threshold value show a more significant deviation against the measured losses, comparing with the modeled losses with threshold surfaces.

With the same identified parameters, the model is excited with rotating inductions in CW and counter CW (CCW) directions. The measured hysteresis losses in CW and CCW reveal a significant difference, mainly caused by BH coils misalignments (Meydan and Zurek, 2006) (Maeda *et al.*, 2007). At high induction, the rotating hysteresis losses begin to decrease as expected. In this work, the maximum flux density, which can be measured under rotating fields, is 1.8 T. The material at this induction is not fully saturated, therefore a hysteresis loss still exists at this flux density.

The simulated rotating hysteresis losses under CW and CCW are identic, which concludes the statement that the differences of hysteresis losses between CW and CCW are caused by measurement errors. The rotating losses versus the magnetization amplitude are depicted in Figure 7. In Figure 7, large deviations between measured losses and the losses simulated with threshold surface can be observed from 1.4 T to 1.7 T, which is similar to the findings presented in Matsuo (2008). The rotating losses derived from the simulation with constant threshold depict a more linear process with respect to the increased flux density.

5. Conclusions

A vector hysteresis stop model with input dependent threshold components is presented in this paper. The isotropic threshold surface is constructed from measured major loop in rolling direction. The four parameters for five hysterons can be identified by minimizing the errors between measured and modeled alternating minor loops.

With the threshold surface, the advanced hysteresis model is able to describe the hysteresis losses and the saturation properties. The rotating measurements are processed in CW and CCW directions. With the same parameters, identified from alternating excitations, the model under rotating excitations is studied. The validation of the vector hysteresis model with measured alternating and rotating hysteresis losses is presented. An improvement of accuracy by representing the saturation properties under alternating and rotating flux densities can be observed in comparison with the simulated losses with constant threshold value.

A further study to improve the anisotropy in magnetic coercive field and the accuracy to represent the rotating losses in the range from 1.4 T to 1.7 T will be carried out.

References

Bastos, J.P.A., Hoffmann, K., Leite, J.V. and Sadowski, N. (2018), "A new and robust hysteresis modeling based on simple equations", *IEEE Transactions on Magnetics*, Vol. 54 No. 3, pp. 1-4, March.

Bavendiek, G., Leuning, N., Müller, F., Schauerte, B., Thul, A. and Hameyer, K. (2019), "Magnetic anisotropy under arbitrary excitation in finite element models", *Archives of Electrical Engineering*, April, Vol. 68 No. 2, pp. 455-466.

Bergqvist, A. (1997), "Magnetic vector hysteresis model with friction-like pinning", *Physica B: Condensed Matter*, Vol. 233 No. 4, pp. 342-347.

Bergqvist, A. and Engdahl, G. (1994), "A phenomenological differential-relation-based vector hysteresis model", *Journal of Applied Physics*, Vol. 75 No. 10, pp. 5484-5486.

Bergqvist, A., Lundgren, A. and Engdahl, G. (1997), "Experimental testing of an anisotropic vector hysteresis model", *IEEE Transactions on Magnetics*, September, Vol. 33 No. 5, pp. 4152-4154.

Bertotti, G. (1998), *Hysteresis in Magnetism (for Physicists, Materials Scientists, and Engineers)*, 1 ed., Elsevier Science, s.l.

Bobbio, S., Miano, G., Serpico, C. and Visone, C. (1997), "Models of magnetic hysteresis based on play and stop hysterons", *IEEE Transactions on Magnetics*, November, Vol. 33 No. 6, pp. 4417-4426.

Chwastek, K. (2013), "Anisotropic properties of non-oriented steel sheets", *IET Electric Power Applications*, August, Vol. 7 No. 7, pp. 573-579.

Krejčí, P. (1996), *Hysteresis, Convexity and Dissipation in Hyperbolic Equations*, Gattötoscho, s.l.

Leite, J.V., Sadowski, N., Kuo-Peng, P. and Bastos, J. (2005), "A new anisotropic vector hysteresis model based on stop hysterons", *IEEE Transactions on Magnetics*, May, Vol. 41 No. 5, pp. 1500-1503.

Maeda, Y., Shimoji, H., Todaka, T. and Enokizono, M. (2007), "Study of the counterclockwise/clockwise (CCW/CW) rotation problem with the measurement of 2-dimensional magnetic properties", *Przeglad Elektrotechniczny*, Vol. 83 No. 4, pp. 18-24.

Martin, F., Singh, D., Belahcen, A., Rasilo, P., Haavisto, A. and Arkkio, A. (2015), "Analytical model for magnetic anisotropy dedicated to non-oriented steel sheets", *The International Journal for Computation and Mathematics in Electrical and Electronic Engineering*, September, Vol. 34 No. 5, pp. 1475-1488.

Matsuo, T. (2008), "Rotational saturation properties of isotropic vector hysteresis models using vectorized stop and play hysterons", *IEEE Transactions on Magnetics*, November, Vol. 44 No. 11, pp. 3185-3188.

Matsuo, T. and Shimasaki, M. (2007), "Generalization of an isotropic vector hysteresis model represented by the superposition of stop models – identification and rotational hysteresis loss", *IEEE Transactions on Magnetics*, March, Vol. 43 No. 4, pp. 1389-1392.

Meydan, T. and Zurek, S. (2006), "Errors in the power loss measured in clockwise and anticlockwise rotational magnetisation. Part 1: mathematical study", *IEE Proceedings - Science, Measurement and Technology*, Vol. 153 No. 4, pp. 147-151.

Torre, E.D., Pinzaglia, E. and Cardelli, E. (2006), "Vector modeling – part II: ellipsoidal vector hysteresis model. Numerical application to a 2D case", *Physica B: Condensed Matter*, February, Vol. 372 Nos 1/2, pp. 115-119.

Xiao, X., Müller, F., Bavendiek, G. and Hameyer, K. (2020), "Analysis of vector hysteresis models in comparison to anhysteretic magnetization model", *The European Physical Journal Applied Physics*, August, Vol. 91 No. 2, p. 20901.

Zhu, L. and Koh, C.S. (2017), "A novel vector hysteresis model using anisotropic vector play model taking into account rotating magnetic fields", *IEEE Transactions on Magnetics*, Vol. 53 No. 6, pp. 1-4.

Corresponding author
Xiao Xiao can be contacted at: xiao.xiao@iem.rwth-aachen.de